Article:
Rashid, A, Vakurov, A and Nelson, A (2018) Phospholipid bilayers at the mercury (Hg)/water interface. Electrochimica Acta, 281. pp. 152-161. ISSN 0013-4686

https://doi.org/10.1016/j.electacta.2018.05.141

Elsevier Editorial System(tm) for Electrochimica Acta

Manuscript Draft

Manuscript Number: EA18-1455R1

Title: Phospholipid bilayers at the mercury (Hg)/water interface

Article Type: Research Paper

Keywords: DOPC bilayers; Hg; negative applied potential; Zn2+ chronoamperometry; electrochemical impedance.

Corresponding Author: Professor laurence andrew Nelson, PhD

Corresponding Author's Institution: university of leeds

First Author: laurence andrew Nelson, PhD

Order of Authors: laurence andrew Nelson, PhD; Alexandre Vakurov; Ashi Rashid

Abstract: This study reports on the electrochemical characterisation of dioleoyl phospatidylcholine (DOPC) bilayer structures on a negatively polarised mercury (Hg) electrode. The bilayers are stable on the Hg surface between -1.0 and -1.3 V applied potential. The experimental approaches were:- (i) Rapid cyclic voltammetry to "fingerprint" the bilayers, (ii) Potential step experiments to record Zn2+ reduction and, (ii) Electrochemical impedance. The results show the following. Both the specific capacitance (5 microF cm-2) and the specific resistance of the bilayer are higher and lower respectively than that of a defect-free free standing DOPC bilayer. This indicates the presence of water and ions in the bilayer within an applied negative field. The bilayer's resistance to electrolyte movement decreases with increase in negative potential to a minimum at - 1.3 V. The DOPC bilayer is less permeable to Zn2+ ions compared to the DOPC monolayer coated electrode at applied negative potentials and its permeability to Zn2+ increases with an increase in negative applied potential. The specific capacitance of the bilayer increases to about 7.5 microF cm-2 with increase in applied negative potential showing the increasing significance of water in the bilayer commensurate with its increased permeability to ions. Adsorption of SiO2 nanoparticles on the bilayer surface causes a step negative potential shift in the anodic capacitance current bilayer reformation peak indicating an acceleration of the bilayer reformation process.

Graphical Abstract (for review)

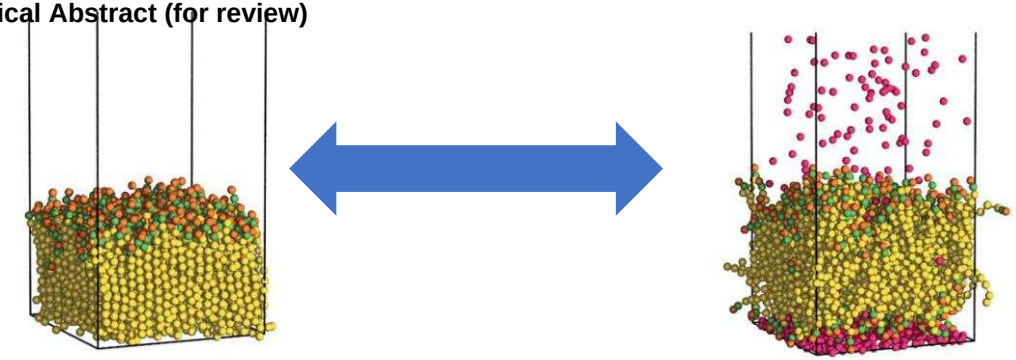

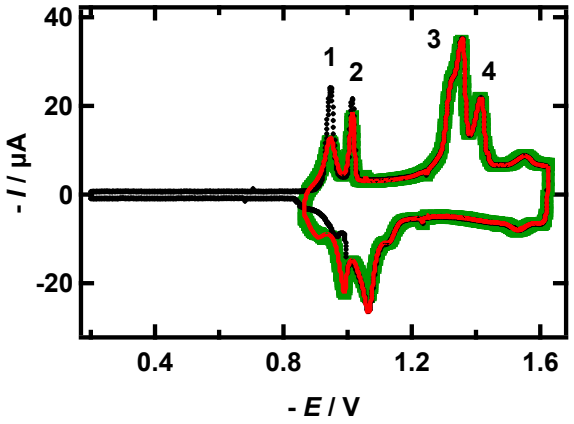

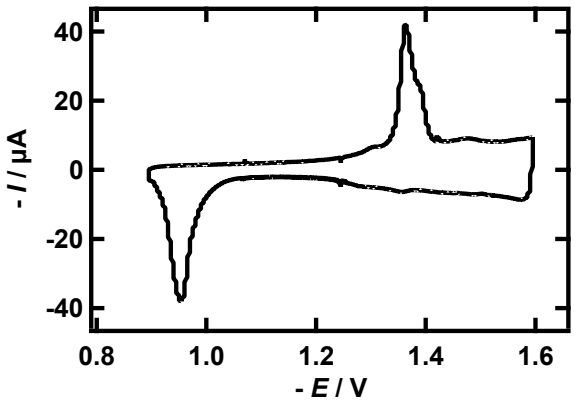

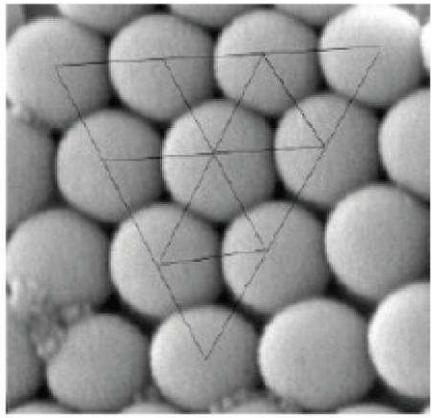

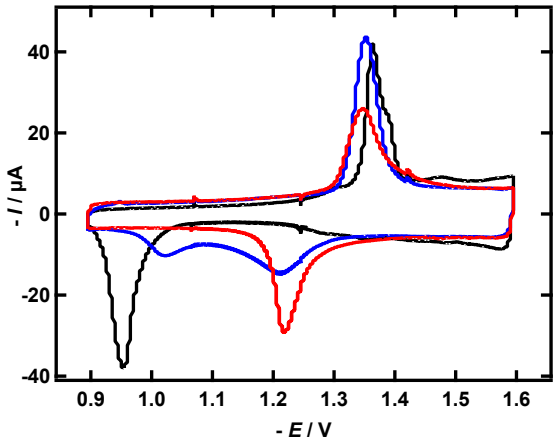

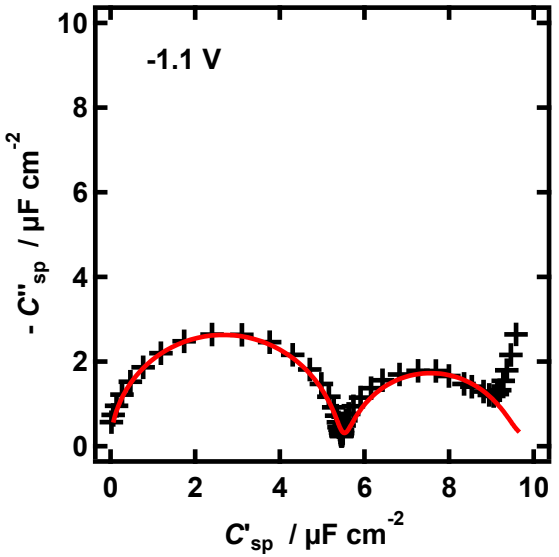

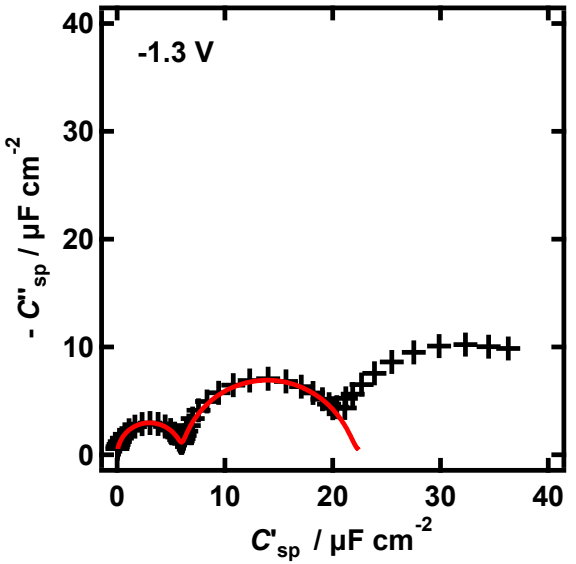

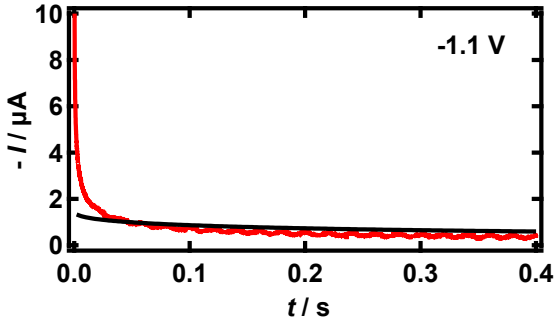

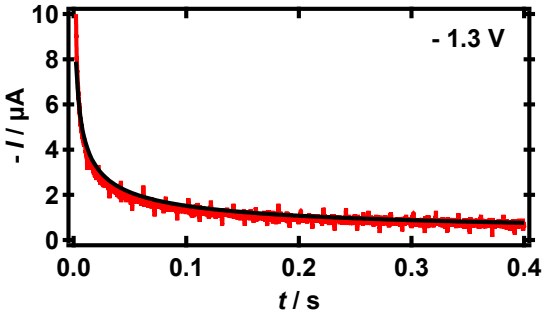

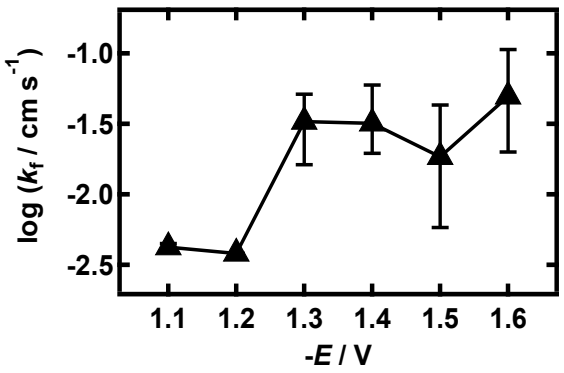

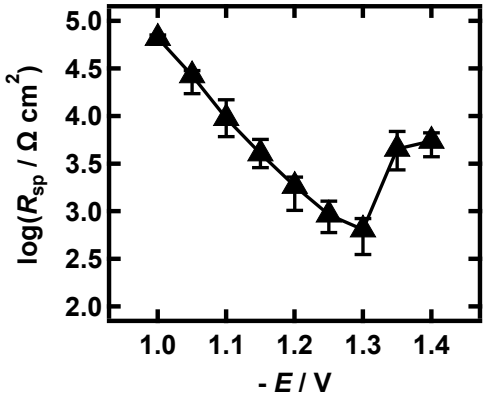

Figure 1

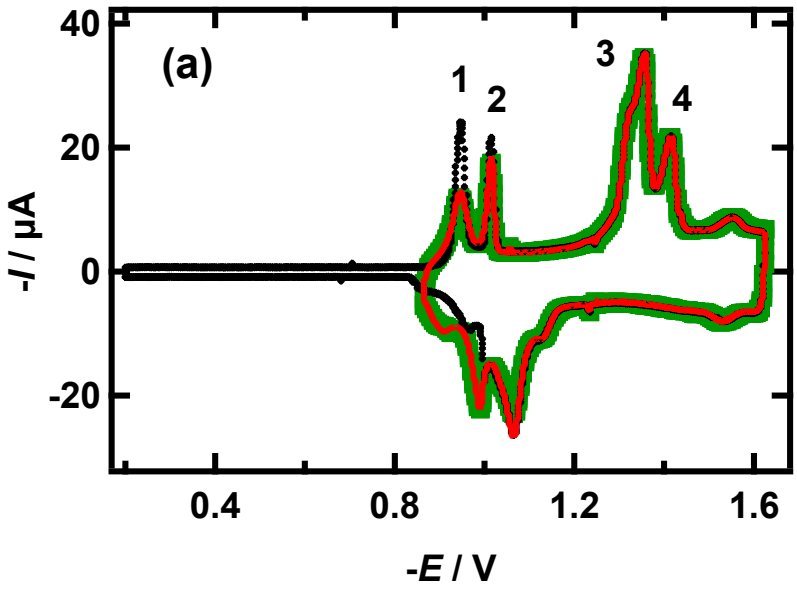
(a)
1
2
3
4
40
20
0
-20
-I / µA
0.4
0.8
1.2
1.6
-E / V

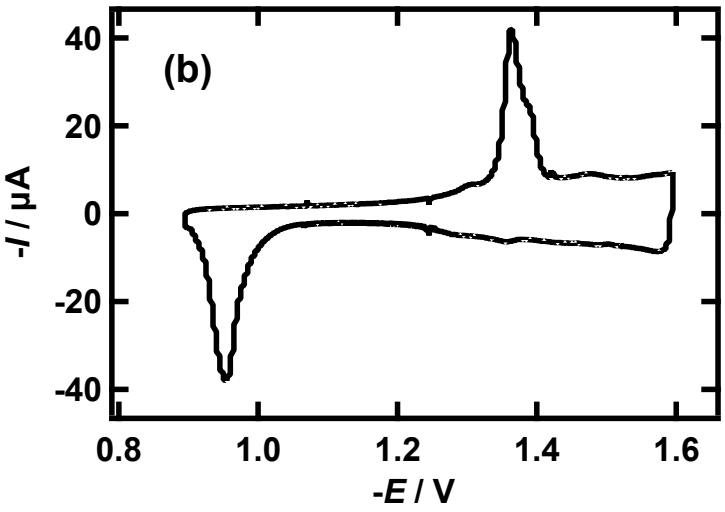
(b)
40
20
0
-20
-40
-I / µA
0.8
1.0
1.2
1.4
1.6
-E / V

Figure 2

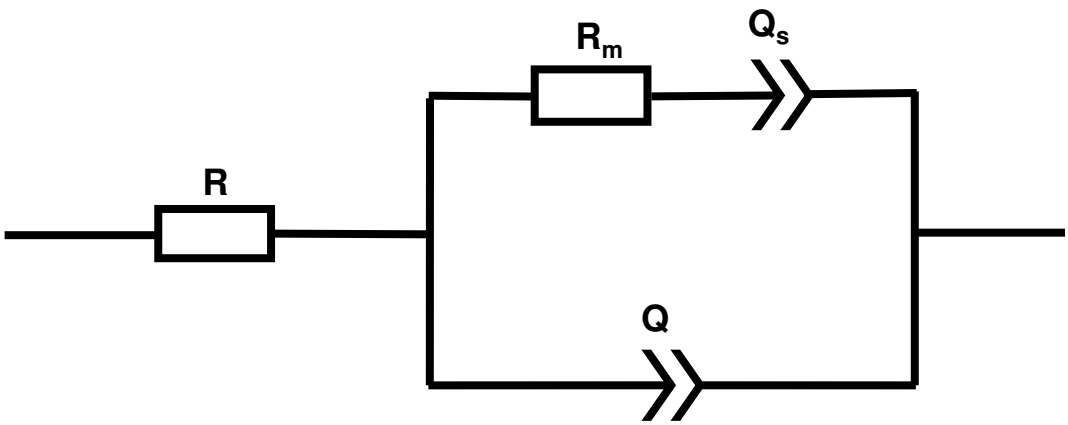

Figure 3

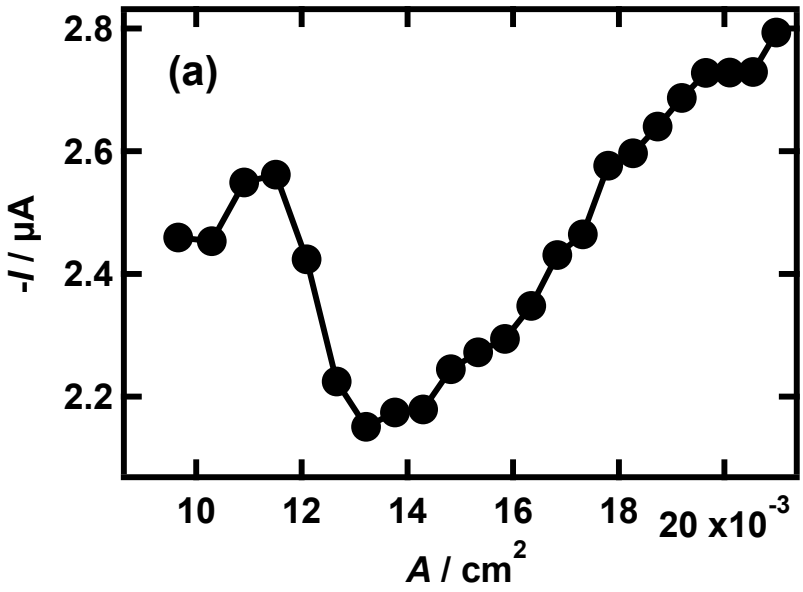
(a)
2.8
2.6
2.4
2.2
-I / µA
10
12
14
16
18
20 x10-3
A / cm2

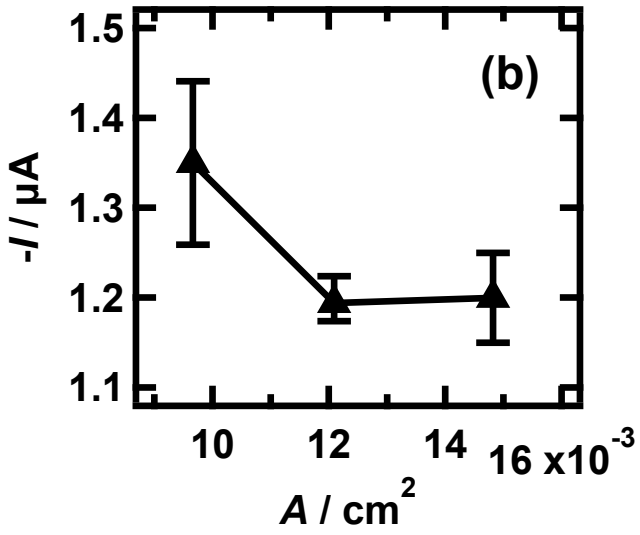
(b)
1.5
1.4
1.3
1.2
1.1
-I / µA
10
12
14
16 x10-3
A / cm2

Figure 4

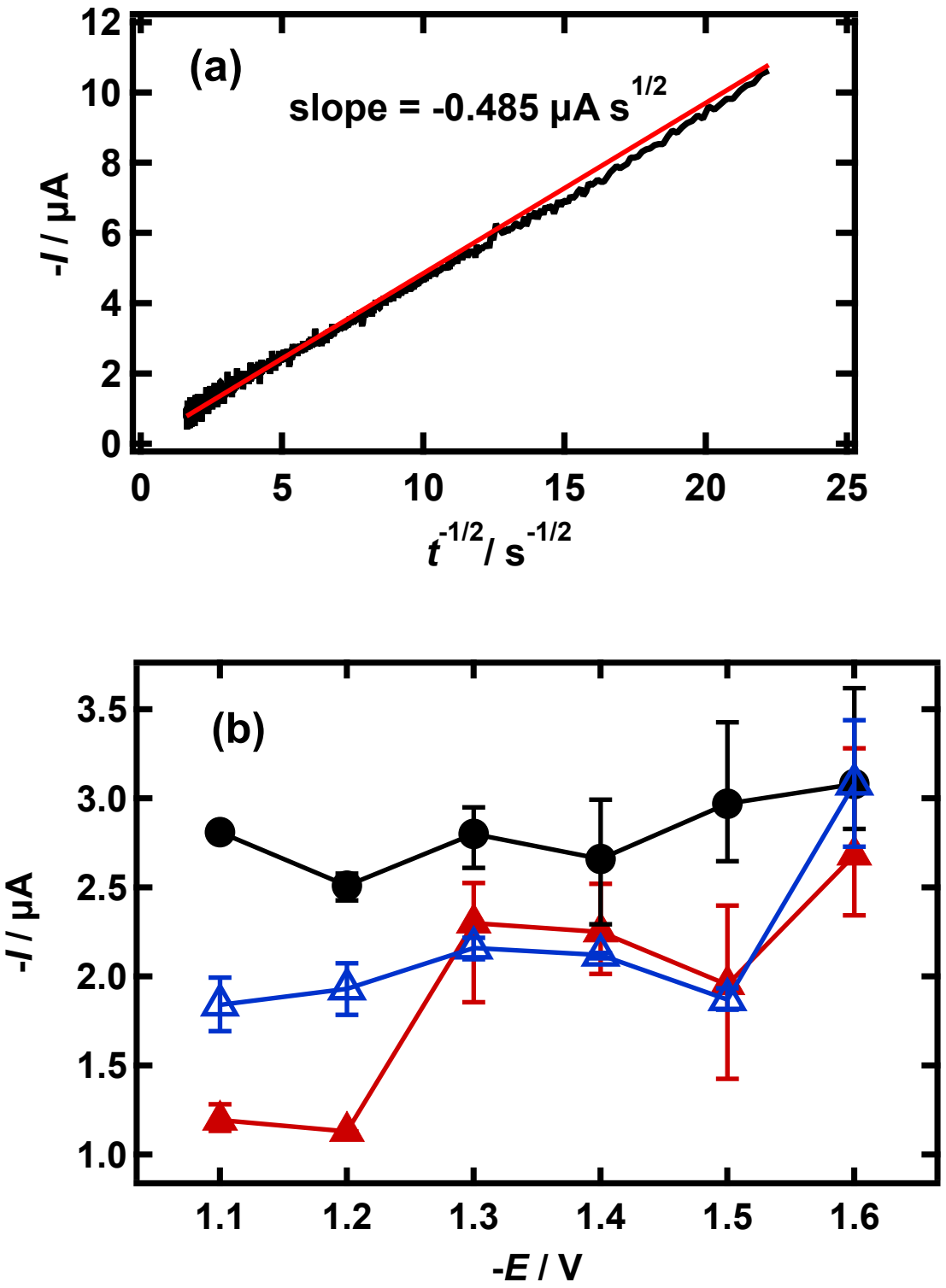
(a)
slope = -0.485 μA s^1/2
-I / μA
t^-1/2 / s^-1/2
0
2
4
6
8
10
12
0
5
10
15
20
25
(b)
-I / μA
-E / V
1.0
1.5
2.0
2.5
3.0
3.5
1.1
1.2
1.3
1.4
1.5
1.6

Figure 5

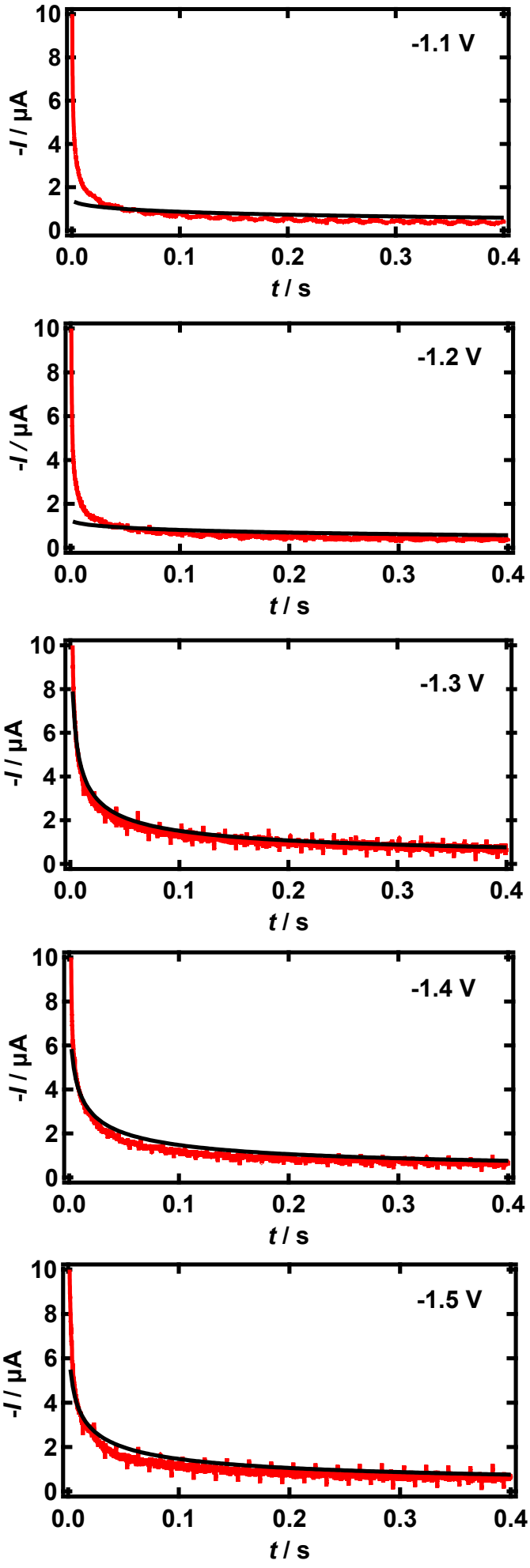

Figure 6

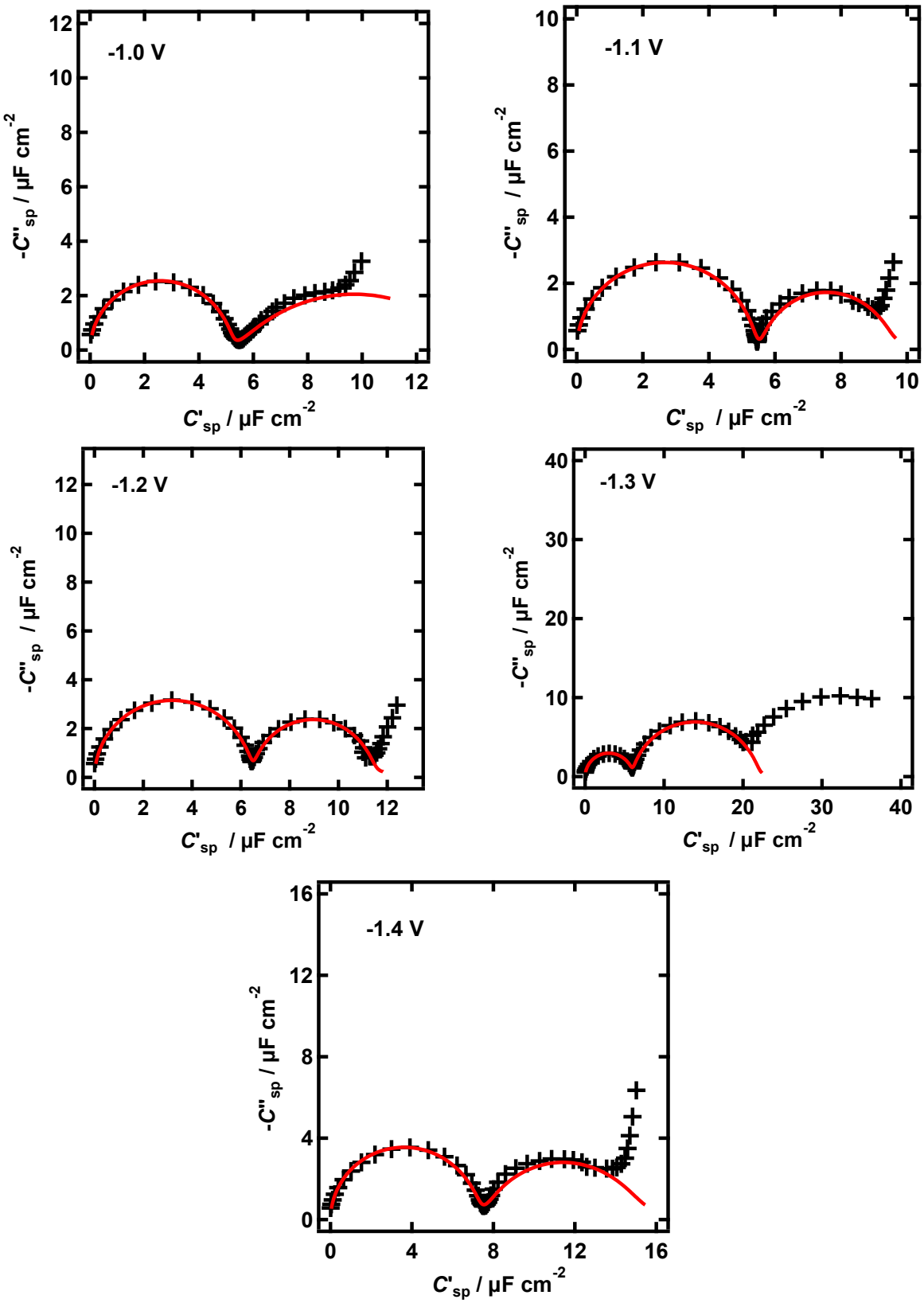

Figure 7

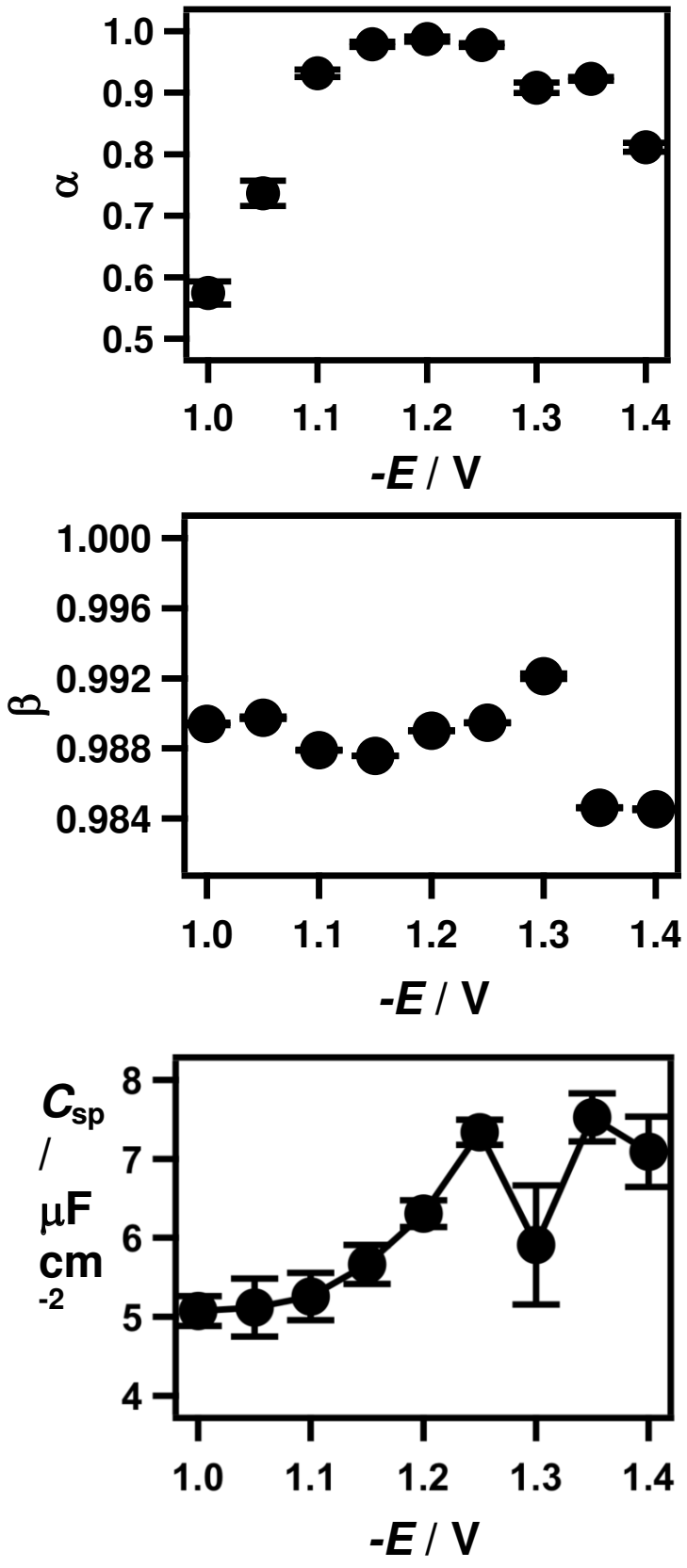
α
1.0
0.9
0.8
0.7
0.6
0.5
1.0
1.1
1.2
1.3
1.4
-E / V
β
1.000
0.996
0.992
0.988
0.984
1.0
1.1
1.2
1.3
1.4
-E / V
C_sp / μF cm^-2
8
7
6
5
4
1.0
1.1
1.2
1.3
1.4
-E / V

Figure 8

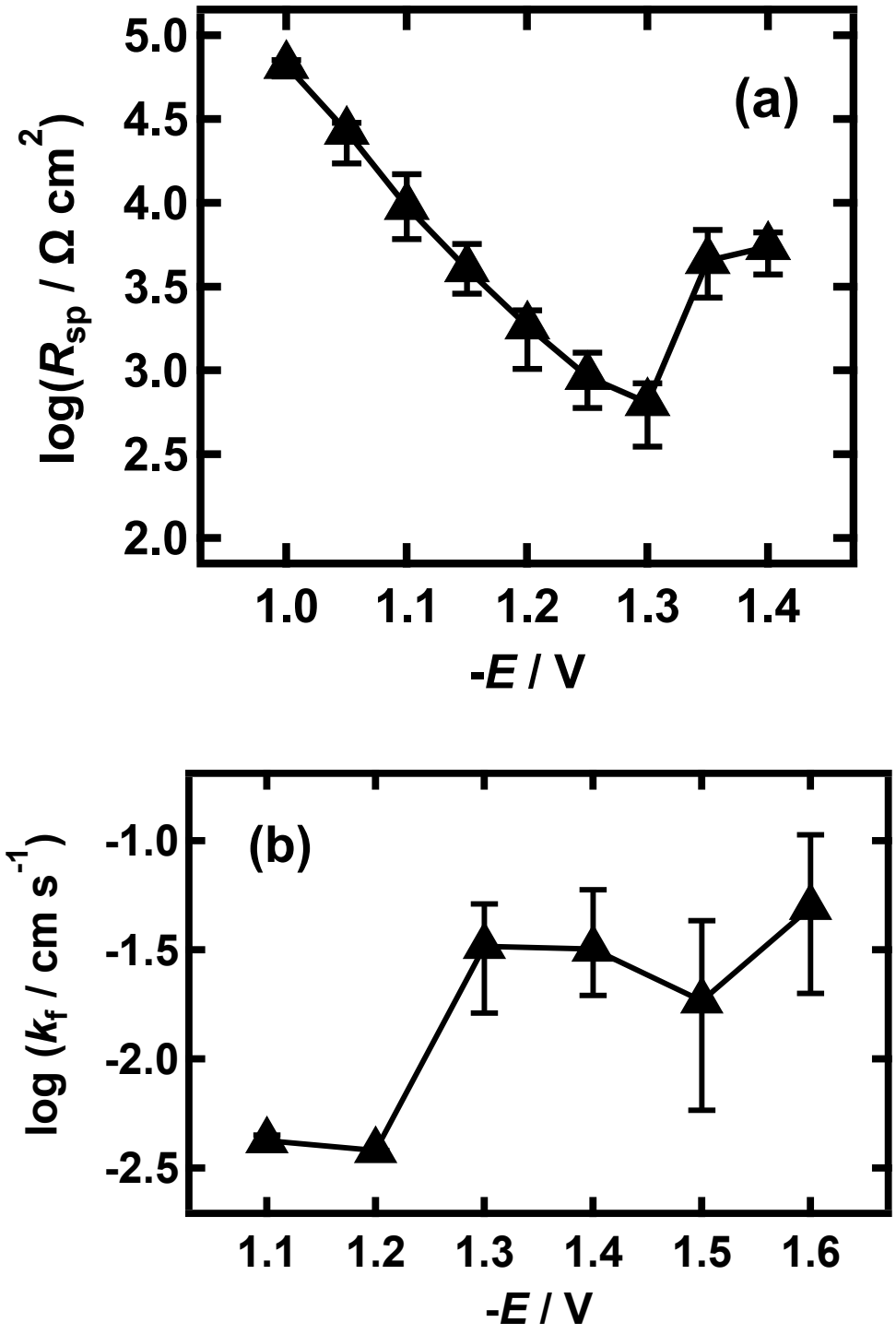
(a)
log(R_{sp} / Ω cm^2)
5.0
4.5
4.0
3.5
3.0
2.5
2.0
1.0
1.1
1.2
1.3
1.4
-E / V
(b)
log (k_f / cm s^{-1})
-1.0
-1.5
-2.0
-2.5
1.1
1.2
1.3
1.4
1.5
1.6
-E / V

Figure 9

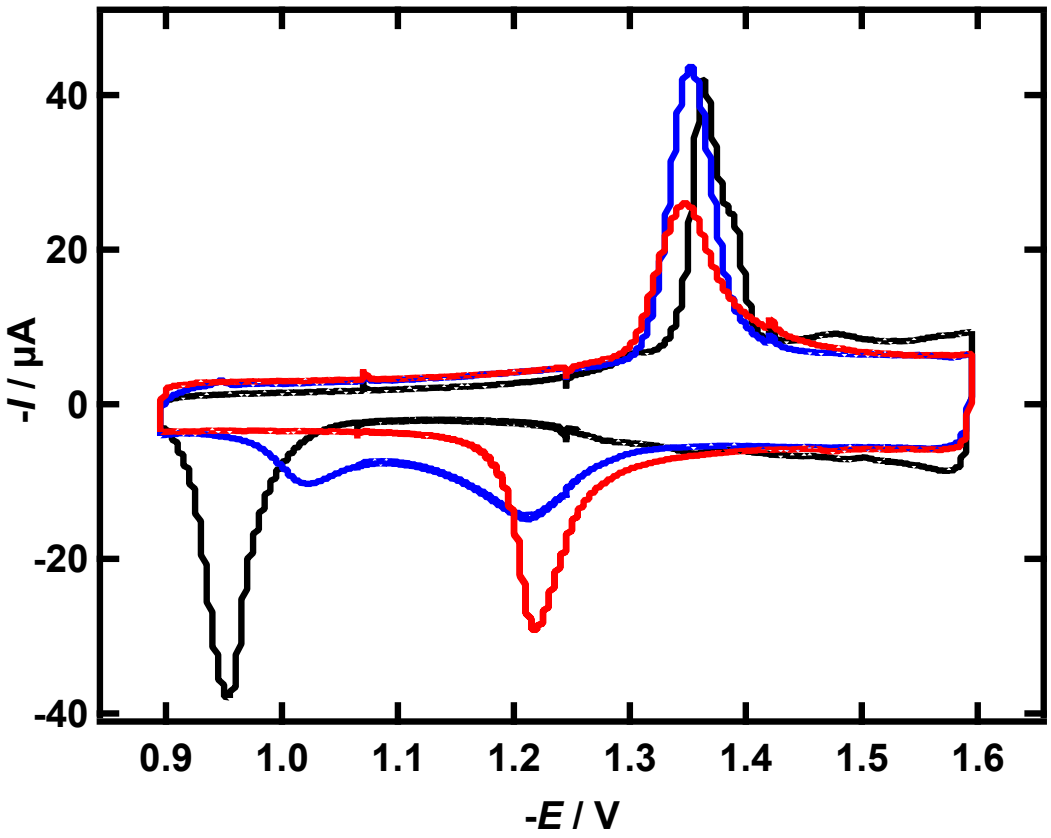

Research Highlights

Stable DOPC bilayers can be deposited on Hg between -0.9 and -1.3 V

Bilayer specific capacitance increases from 5 to 7.5 μF cm^{-2} between -1.0 to -1.3 V

Extra capacitative element identified with movement of electrolyte in bilayer pores

Resistance decreases and Zn^{2+} permeability increases between -1.0 and -1.3 V

SiO_2 adsorbs on bilayer and accelerates bilayer reformation on anodic scan

Phospholipid bilayers at the mercury (Hg)/water interface

Ashi Rashid[a], Alexandre Vakurov and Andrew Nelson*

[a]present address, University of Engineering and Technology, Lahore, Pakistan.

*corresponding author, a.l.nelson@leeds.ac.uk

School of Chemistry, University of Leeds, Woodhouse Lane, LS9 2JT, Leeds, UK

Abstract

This study reports on the electrochemical characterisation of dioleoyl phospatidylcholine (DOPC) bilayer structures on a negatively polarised mercury (Hg) electrode. The bilayers are stable on the Hg surface between -1.0 and -1.3 V applied potential. The experimental approaches were:- (i) Rapid cyclic voltammetry to "fingerprint" the bilayers, (ii) Potential step experiments to record Zn^{2+} reduction and, (ii) Electrochemical impedance. The results show the following. Both the specific capacitance (5 μF cm^{-2}) and the specific resistance of the bilayer are higher and lower respectively than that of a defect-free free standing DOPC bilayer. This indicates the presence of water and ions in the bilayer within an applied negative field. The bilayer's resistance to electrolyte movement decreases with increase in negative potential to a minimum at -1.3 V. The DOPC bilayer is less permeable to Zn^{2+} ions compared to the DOPC monolayer coated electrode at applied negative potentials and its permeability to Zn^{2+} increases with an increase in negative applied potential. The specific capacitance of the bilayer increases to about 7.5 μF cm^{-2} with increase in applied negative potential showing the increasing significance of water in the bilayer commensurate with its increased permeability to ions. Adsorption of SiO_2 nanoparticles on the bilayer surface causes a step negative potential shift in the anodic capacitance current bilayer reformation peak indicating an acceleration of the bilayer reformation process.

Keywords, DOPC bilayers; Hg; negative applied potential; Zn^{2+} chronoamperometry; electrochemical impedance.

1. Introduction

Model lipid bilayers have been investigated extensively over the past few decades to develop an understanding of the properties and function of biomembranes. These model lipid bilayers vary from free standing vesicles [1] to free-standing bilayers [2] to bilayers supported on various solid substrates such as gold [3,4] and mica [5,6] directly or via linkers. Using mercury (Hg) as a substrate, tethered lipid bilayers have been developed and investigated using different tethering materials such as alkanethiols [7-13], polymers [14] and peptides [15]. Only monolayers of phospholipid adsorb on Hg at potentials around the position of zero charge (PZC) of ~ -0.4 V vs Ag/AgCl [16]. The potential dependent formation of a dioleoyl phosphatidylcholine (DOPC) bilayer on the surface of Hg at the electrolyte interface has been reported recently at applied potentials more negative than -0.9 to -1.0 V due to favourable energetics [17] and is consistent with physicochemical and thermodynamic predictions [18,19]. This DOPC bilayer on Hg was characterised using rapid cyclic voltammetry (RCV) and atomic force microscopy (AFM) [17]. Using RCV, the DOPC bilayer on Hg has been shown to exhibit a constant low capacitance region from -1.0 V to -1.3 V followed by a sharp, well-defined cathodic capacitance current peak due to the breakdown of the bilayer at about -1.3 V. A reverse anodic process is represented by an anodic capacitance current peak showing marked hysteresis [17]. These bilayers are stable in the potential domain from -1.0 V to -1.3 V and are unstable at more positive potentials than -0.9 V due to a spontaneous conversion to a monolayer. AFM studies have shown that the thickness of the bilayer is 6.5 to 7 nm with 95 % coverage in voltage range from -1.0 V to -1.35 V decreasing to 2.5 to 3 nm following the cathodic capacitance current peak at higher negative potentials without a change in coverage [17]. The reverse process is observed by the AFM study as bilayer reformation.

This present investigation aims to characterise these bilayers electrochemically in a more detailed manner using Zn^{2+} reduction at, and electrochemical impedance of, the bilayer coated Hg surface. This is the first study to our knowledge which reports on the electrochemical characterisation of a

DOPC bilayer structure directly and non-covalently supported on the surface of the Hg electrode. Non-covalently bound bilayers are a significant advance to tethered bilayers since they more closely represent the biomembrane structure with symmetrical conformation allowing free mobility of the phospholipid on the ultra-smooth Hg.

2. Experimental

2.1. Materials and methods

The electrolyte, KCl (0.1 mol dm^{-3}) was prepared from KCl (Fisher Chemicals Ltd.) calcined at 600 ^{o}C in a muffle furnace and dissolved in 18.2 MΩ MilliQ water containing 0.001 mol dm^{-3} phosphate at pH 7.4 and was used in all the experiments except for the Zn^{2+} reduction studies where phosphate was not added to avoid precipitation of Zn (II) in the electrolyte solution. For the Zn^{2+} reduction experiments, $ZnCl_2$ (Sigma Aldrich) was employed to prepare a 0.2 mol dm^{-3} stock solution using 18.2 M Ω MilliQ water. The electrolyte solution was purged with argon gas for 15 to 20 minutes prior to experiment. After deaeration, a blanket of argon gas was maintained above the fully deaerated solution to avoid penetration of any oxygen into the solution during all experiments. A DOPC solution (Avanti Lipid) of 2.54 mmol dm^{-3} was prepared in pentane (HPLC grade, Fisher Scientific Chemicals Ltd.) in a clean glass vial and was stored at -20 ^{o}C. A glass syringe was used to transfer the lipid solution to the electrolyte surface in the electrochemical cell. 15 μL of this stock DOPC solution was spread at the argon-electrolyte interface in the electrochemical cell [20,21]. A period of about 5 to10 minutes was required for the pentane to evaporate. A Kemula-type (Polish Academy of Sciences, Warsaw,Poland) hanging Hg drop electrode (HMDE) was used for the experiments and was lowered through the lipid-electrolyte surface slowly allowing DOPC deposition. Accordingly it was coated with a fresh DOPC layer prior to each series of experiments. The electrochemical cell, counter and reference electrodes and all other glass apparatus were treated and washed with piranha solution between experiments to remove organic contamination. The

apparatus and the electrodes were then rinsed with MilliQ water to remove any piranha residue since the presence of trace piranha in the electrolyte can damage the lipid.

2.2. Electrochemical set-up

The experiments were performed in a standard three electrode cell using a Ag/AgCl electrode as reference electrode with a porous sintered glass frit separating the inner 3.5 mol dm^{-3} solution of reference electrode from the outer electrolyte solution and a Pt rod as a counter electrode. All potentials in the text are referred to the potential of this electrode. The electrochemical apparatus was contained in a Faraday cage. RCV measurements were carried out with a PGSTAT 30 Autolab potentiostat (Ecochemie, Utrecht, Netherlands) interfaced to a PowerLab 4/25 signal generator (AD Instruments Ltd.) controlled by Scope software. The potential step measurements were carried out using the Autolab system, GPES (General purpose electrochemical software) with PGSTAT 30 and controlled with Autolab software. The integrity of the DOPC bilayer was checked at the beginning and end of each experiment by RCV. The Autolab system frequency response analyser (FRA) with PGSTAT 30 was used for the impedance measurements. The impedance data were transformed to the complex capacitance plane and fitted to an analytical model as described below.

2.3. Electrochemical techniques

2.3.1. Rapid cyclic voltammetry (RCV)

RCV was used as the technique to characterise the DOPC bilayers on Hg and to probe the properties of the bilayer by recording a fast scan "fingerprint" at a scan rate (ν) of 40 Vs^{-1}. The following scanning programme was used. A RCV triangular waveform was generated whereby the applied voltage excursion was taken from -1.25 to -1.6 V followed by a return to -0.9 V and then to -1.25 V where a short waiting period corresponding to the time of the sawtooth excursion was maintained. Bilayers can be formed in two ways:- (a) conversion of a phospholipid monolayer supported on a HMDE electrode to a bilayer by decreasing the area of electrode and, (b) direct

deposition from electrolyte surface, scanning the HMDE between potentials between -0.9 and -1.6 V at 40 Vs^{-1}. To fully characterise a DOPC bilayer, a DOPC monolayer was deposited on an electrode of > 0.02 cm^2 area within the potential scanning regime of -0.2 to -1.6 V. Subsequently, the potential scanning programme was switched to -0.9 V to -1.6 V. In this potential domain, the monolayer exhibited the phase transitions characterised by the capacitive current peaks on the voltammogram [22,23] of a monolayer (see Figure 1(a)). The area of the HMDE is then decreased in a controlled fashion to ~ 55% of its initial value. The evidence for this decreased area electrode supporting an "equilibrium" bilayer structure is discussed in the results section. In the bulk of the experiments, the HMDE was lowered through the DOPC layer at the electrolyte surface scanning the HMDE between potentials -0.9 and -1.6 V at 40 Vs^{-1}. Subsequent RCV using the potential programme described above established the characteristic RCV scan of a bilayer on Hg (Figure 1(b)). All RCV currents were normalised to electrode area 0.0088 cm^2.

2.3.2. Potential step experiments

Potential step experiments were carried out to investigate the interference of the DOPC bilayer supported on HMDE to the Zn^{2+}/Zn(Hg) electrode process at different applied negative potentials. The basic principle of the Zn^{2+} reduction experiments is that the suppression of the electrochemical reduction of Zn^{2+} by the DOPC bilayer is due to the lower permeability of the DOPC layer coating and thus restricted access of Zn^{2+} ions to the Hg surface. The following procedure was used. Following de-aeration of the electrolyte, the DOPC bilayer was deposited on the electrode surface and a "fingerprint" RCV was recorded. Subsequently 25 μL of the stock Zn^{2+} solution was added to 25 mL of electrolyte and stirred for 30 s to give 0.2 mmol dm^{-3} Zn^{2+} concentration. Potential pulses were initiated from -0.85 V (at the base of the Zn^{2+} reduction wave) to potentials from -1.2 to -1.5 V and the corresponding current transients were recorded in quiescent solution and current sampled at 30 ms to construct sampled current voltammograms. The standard redox potential of the Zn^{2+}/Zn(Hg) couple is -0.97 V [24] and transients were therefore recorded in the limiting current

region of Zn^{2+} reduction. After the pulsing programme had been performed, an RCV scan was recorded to ensure that the phospholipid bilayer had not degraded during the experiment. Identical experiments were performed at a DOPC monolayer coated and uncoated Hg electrode. All currents regardless of electrode area were normalised to an electrode area of 0.0088 cm^2. The current transients (I(t)) from potential step experiments at uncoated Hg in the presence of Zn^{2+} in solution were fitted to the Cottrell equation [24];

$$I(t) = nFAD^{1/2} c / \pi^{1/2} t^{1/2} \qquad [1]$$

where n is the number of electrons transferred in the redox reaction, F is the Faraday's constant (96500 coulomb mol^{-1}), A is the area of electrode, c is the concentration of Zn^{2+} in electrolyte solution, D is the diffusion constant of Zn^{2+} and t the time since pulse initiation. The slope of the Cottrell plots was used to calculate the diffusion constant of Zn^{2+}. In addition, a kinetic analysis of the reduction of Zn^{2+} to Zn (Hg) at the bilayer coated electrode was performed using the equations defining an irreversible reduction of an electroactive species at a planar [25] electrode and the rate constant (k_f) was determined using the following equation;

$$I(t) = nFAk_f c \exp (k_f^2 t/D) \ \text{erfc} (k_f t^{1/2}/D^{1/2}) \qquad (2)$$

where k_f represents a heterogeneous rate constant characterising the irreversible reduction of Zn^{2+}. Because of the restricted access of Zn^{2+} to the Hg surface caused by a DOPC bilayer, we identify k_f with the permeability of the Zn^{2+} in the bilayer coated electrode.

2.3.3. Electrochemical impedance

Impedance (Z) versus frequency (f) measurements were carried out at the HMDE electrode coated with DOPC bilayer using frequencies logarithmically distributed from 65,000 to 0.1 Hz, with ac amplitude (ΔV) 0.005V at potentials from -1.0 to -1.5 V. The experimental conditions for the measurement of impedance were used exactly as described previously [26]. The impedance data were transformed to the complex capacitance plane and were expressed as imaginary ($-C''_{sp} = Y'\omega^{-1}_{sp}$) and real ($C'_{sp} = Y''\omega^{-1}_{sp}$) specific capacitance which are the respective imaginary and real

capacitance values (-C'' and C') divided by the electrode area and are experimental values calculated from the experimental impedance measurements. Note that Y'' and Y' are the imaginary and real admittance values respectively and ω is the angular frequency which equals 2πf. The values of $-C''_{sp}$ which are plotted against C'_{sp} in the complex capacitance plane for all values of frequency [26] always yield a single semicircle corresponding to the resistance-capacitance (RC) element with no frequency dispersion for a series RC circuit containing an ideal capacitor. Indeed when a DOPC monolayer is supported on a Hg electrode it behaves as a simple capacitor at the position of zero charge (PZC) of Hg [26]. Any imperfections in the monolayer following interactions with adsorbed/penetrated compounds [26,27] and ions [28] and phase transitions [20,26] appear as an extra capacitative element in the complex capacitance plot [20,26-28]. In this study, the results of the impedance measurements are therefore considered in terms of the properties of the phospholipid bilayer as compared to the DOPC monolayer which are already well known [20,26-28].

2.3.4. Impedance model

The impedance data of DOPC coated electrodes were fitted using IGOR (Wavemetrics) to eqn [3] below in the same way as described previously [20,26-28].

$$Y = 1/\{R + [(i\omega)^{\beta}((Q_s\text{-}Q)/1 + (i\omega\tau)^{\alpha}) + Q]^{-1}\} \qquad [3]$$

where Y is admittance, R is the uncompensated solution resistance, τ is relaxation time constant of the additional capacitative element. α represents the distribution of values of τ around the most probable value (= or < 1) and β is a coefficient which is equal or < 1 and has been shown to be inversely related to the homogeneity of the lipid layers [20,26-28]. Q_s and Q are constant phase element (CPE) constants, Q_s-Q is the CPE constant for the additional low frequency or capacitative element. All data obtained from the bilayer impedance experiments were fitted to eqn (3). The six parameters: Q, Q_s-Q, α, β and τ were obtained from the subsequent curve fitting of the $-C''_{sp}$ and C'_{sp} versus log ω plots respectively. The mean of the extracted coefficients or fit parameters (α, β,

Q_s-Q, Q and τ) are used to calculate values for -C''$_{sp}$ and C'$_{sp}$ at respective frequency values which are then plotted as fits to the experimental -C''$_{sp}$ versus C'$_{sp}$ plots. The capacitance values: C_s - C and C are derived from Q_s-Q and Q according to Sluyter's equation [29] as before [30] as follows:

$$C = [Q R^{(1-\beta)}]^{1/\beta} \qquad [4]$$

$$C_s - C = (Q_s - Q)\,\tau^{(1-\beta)} \qquad [5]$$

C is identified as the zero frequency capacitance (ZFC) of the bilayer and C_s-C is the capacitance of the additional low frequency capacitative element. The errors stated for these coefficients are treated according to the error propagation rule for a mean function. Note that eqn (5) is derived from eqn (4) treating the capacitance of the additional capacitative element in the same way as the double layer capacitance. Following the extraction of the value of the additional capacitative element (C_s-C) of the data, the resistance of this element can be obtained [30] since $R_m/\tau=(C_s-C)$. This resistance relates to the displacement of charge during the relaxation of the element. In this paper the specific resistance R_{sp} is defined as R_m multiplied by the electrode area. Figure 2 shows the equivalent circuit representing eqn [3] with symbols as described above containing the equivalent circuit for a dielectric relaxation [31] and Constant Phase Element Q_s replacing capacitor.

3. Results

3.1. Bilayer formation

A DOPC monolayer assembled on Hg electrode displays two distinctive capacitance current peaks 1 and 2 at -0.94 and -1.0 V respectively in response to the application of a negatively increasing applied potential (Figure 1(a)). These capacity current peaks represent two consecutive phase transitions occurring in the monolayer. The capacitance current peak 1 relates to electrolyte ingression into the monolayer and capacitance current peak 2 corresponds to the transformation of

a porous monolayer to bilayer patches as established both experimentally and theoretically in previous work [17-20]. Further broad capacitance current peaks 3 and 4 which occur at higher negative potentials (-1.25 to -1.3V respectively) are shown to lead to structures with a thickness three times of that of a monolayer which indicate the formation of semi-liposomal conformations [17]. These structures collapse to a monolayer at more negative potentials. The appearance of the RCV capacitance current peaks characteristic of the DOPC monolayer during a negative potential excursion from -0.9 and -1.6 V indicates the presence of a monolayer (Figure 1(a)). As a result, it should be possible to stabilise a continuous bilayer on the Hg surface in the potential region negative to that characterising capacitance current peak 2. Indeed, a decrease in the monolayer coated electrode area initiates bilayer formation which is marked by a progressive suppression of capacitance current peaks 1 and 2 leading to a complete suppression of these two capacitance current peaks and the formation of a flat low capacitance region at these potentials and a fusion of the capacitance current peaks 3 and 4 (Figure 1(b)).

In the RCV of the bilayer, the cathodic capacitance current peak in the bilayer RCV is reversed on the anodic scan but with considerable hysteresis (Figure 1(b)). From the previous paper [17] the cathodic capacitance current peak is shown to indicate a breakdown of the bilayer structure and the anodic capacitance peak current corresponds to bilayer reformation. Figure 3(a) displays the effect of gradual and consistent decrease in electrode area on the area normalised capacitance current at -1.07 V during the transformation of the DOPC monolayer to bilayer on the surface of HMDE. The area normalised capacitance current decreases to a minimum which also corresponds to the lowest permeability to Zn^{2+} reduction current (Figure 3(b)) and presumably represents the most ordered DOPC bilayer configuration. We call this the “equilibrium” bilayer conformation. The DOPC bilayer, for which the area of the electrode is decreased by 0.55 of the initial electrode area (Figure 3(b)), exhibited this lowest, area normalised, capacitance current value. This was the procedure used to characterise the formation of a bilayer. Subsequent to these experiments, the

electrode was expanded back to the original area to observe any changes in the monolayer due to loss of lipid to the capillary walls or electrolyte solution due to contraction of the lipid coated electrode. It can be seen from Figure 1(a) that the capacitance current-potential plots before (red) and after (green) the changes to the electrode area are identical showing that the lipid remains intact on the electrode surface during the course of experiments. Later experiments showed that direct deposition of a bilayer on the electrode is possible by lowering the electrode through the DOPC on the electrolyte surface when the electrode is scanned at potentials between -0.9 and -1.6 V at 40 Vs^{-1}. This bilayer was characterised by RCV as above. This second method of deposition was employed during the bulk of the bilayer experiments.

3.2. Zn^{2+} reduction

The DOPC monolayer on a Hg electrode has been found to be conductive to ions in the potential range of -0.9 to -1.6 V [32]. The reduction of Zn^{2+} at the uncoated Hg electrode surface exhibited Cottrellian behaviour as a linear fit to I(t) vs $t^{-1/2}$ plots (Figure 4(a)). The diffusion constants for the diffusion of Zn^{2+} ion from bulk of electrolyte solution to the uncoated Hg is calculated from the slope of the plots at -1.1 V as ~ 6.4 x 10^{-6} cm^2 s^{-1}. This value is lower than the value of 6.73 x 10^{-6} [33] and 7.03 [34] cm^2 s^{-1} but is used in all the kinetic analysis in this paper. Figure 4(b) shows the sampled current voltammograms of Zn^{2+} at 30 ms for the bilayer deposited on Hg. For uncoated Hg, the current remains effectively constant at potentials -1.1 to -1.6 V varying between -2.5 to 3.0 μA. The Zn^{2+} reduction current at a DOPC monolayer coated electrode is lower and is 1.75 μA at -1.1 V increasing between potentials -1.5 and -1.6 V to the reduction current at an uncoated electrode. The Zn^{2+} reduction current at the DOPC bilayer coated electrode is predictably less (1.2 μA) compared to the uncoated Hg and DOPC monolayer coated Hg electrode at potentials -1.1 to -1.2 V (Figure 4 (b)). An increase in Zn^{2+} reduction current at the bilayer coated electrode occurs between potentials -1.2 to -1.3 V and indicates an increase in permeability of the DOPC bilayer to Zn^{2+}.

The current for Zn^{2+} reduction at the bilayer surface is decreased due to the covered surface introducing a kinetic element into the electron transfer process. Since the Zn^{2+}/Zn(Hg) exchange process at the uncoated Hg surface in 0.1 mol dm^{-3} ionic strength is relatively facile (standard heterogenous rate constant, k^0, =2.3 x 10^{-2} cm s^{-1} [35]), this kinetic element in the reduction relates to the permeability of Zn^{2+} in the bilayer. The current-time (I(t) vs t) data for the DOPC bilayer is fitted to the equation of an irreversible reduction of an electroactive species at a planar electrode described in eqn (2). Electrode planarity is assumed due to the short time scales (0.4 s) of the transients. Fig 5 shows the I(t) vs t transients of the DOPC bilayer at the applied potentials (-1.1 to -1.5 V) together with the corresponding fits to eqn [2]. Qualitatively it can be seen that with increase in negative potential, a current increase is noted at medium to longer times of the transient and this is shown in the sampled-current voltammograms at 30 ms into the pulse in Fig 4(b). In addition it can be also observed that the model described by eqn [2] does not fit the I(t) vs t dependence at less negative potentials (-1.1 and -1.2 V) at short time scales (<30 ms) but the fit to the current transient is improved for the whole transient at more negative potentials (-1.3 to -1.5 V). Nonetheless an irreversible rate constant for Zn^{2+} reduction at the bilayer coated electrode was extracted from the fits and is plotted against potential and discussed later in this paper. The initial spike in Zn^{2+} reduction at less negative potentials can be related to a relaxation of bilayer structure from more permeable to less permeable state following the initiation of the pulse at -0.85 V.

3.3. Impedance studies

The model described in eqn [3] is applied to the impedance data derived from the "equilibrium" DOPC bilayer on Hg at different potentials consistent with the existence of bilayer. This model is fitted to the $-C''_{sp}$ and C'_{sp} versus log ω plots in the complex capacitance plane as displayed in Figure 6. The high frequency semicircle corresponds to the RC charging process of the DOPC bilayer on Hg [20,26-28]. The second semicircle becomes increasingly resolved and significant

(Figure 6) as the applied negative potential is increased. Figures 7(a) and 7(b) summarise the variation in α and β respectively extracted from the fitting of experimental impedance data to eqn [3] for the DOPC bilayer with changes in applied potential. An increase in the α value to close to 1 on increasing the applied negative potential indicates an increase in significance of the relaxation with a time constant, τ, which decreases from 550, 52, 10 to 11 ms, at -1.0, -1.1, -1.2 and -1.3 V respectively with minimum dispersion in value. The relatively low time constant and its discrete value ($\alpha \sim 1$) is characteristic of ionic/water movement and non-Debye type relaxations within the bilayer [28,31]. We identify therefore the additional capacitative element as representing the movement of electrolyte in the bilayer and R_m as the bilayer resistance to this movement. For any movements or changes involving lipid molecules, τ values would be more dispersed with α significantly less than 1 and β less than 1 to indicate structural changes. Indeed a third lower frequency relaxation is evident at -1.3 V (see Figure 6) and coincides with the onset of the capacitance current peak representative of the bilayer breakdown process. The β value remains almost constant or increases only slightly with an increase of the negative potential to -1.3 V. At more negative potentials, a step decrease in β can be related to the onset of the capacitance current peak representative of the bilayer breakdown process and consequent increase in roughness. C_{sp} which is the zero frequency capacitance (ZFC) [26-28] is nearly constant at ~5 μF cm^{-2} between the potential -1.0 and -1.1 V and increases to ~7.5 μF cm^{-2} at -1.25 V (Figure 7(c)).

Figure 8(a) displays the value of the bilayer specific resistance R_{sp} derived from the impedance analysis which can be compared with the k_f for Zn^{2+} reduction (see Figure 8(b)) at the bilayer coated electrode both plotted versus potential. Notably the membrane resistance, R_{sp}, to electrolyte decreases with increase in applied negative potential but at -1.3 V which characterises the onset of the bilayer breakdown process the value of R_{sp} increases presumably because a denser monolayer is formed as shown by the AFM study [17]. k_f which in reality is a record of the permeability of the bilayer to Zn^{2+} ions at longer time scales (> 20-30 ms) also increases from potentials -1.2 to -1.3 V

indicating an increase in bilayer permeability to Zn^{2+} but levels off and decreases somewhat from -1.4 to –1.5 V.

3.4. Interaction of SiO_2 particles with the DOPC bilayer.

Figure 9 displays the RCV capacitance current - potential plots of the DOPC bilayer on Hg in the presence and absence of 0.00125 % of Ludox SM-30 14 nm [36,37] amorphous silica nanoparticles in the electrolyte solution at different exposure times. The DOPC bilayer/SiO_2 interactions result in the suppression of the capacitance current peak on the cathodic scan in addition to a split and then step negative shift of capacitance current peak on the anodic scan. The shift in capacitance peak on the anodic scan to higher negative potentials indicates the shortening of the onset of the reverse process and a decrease in the hysteresis between the cathodic and anodic processes.

4. Discussion

The lowest value of specific capacitance of the DOPC bilayer on Hg is 5 μF cm^{-2}. The specific capacitance of a DOPC monolayer on Hg is 1.80 μF cm^{-2} [32] which roughly corresponds to the defect-free monolayer apolar fraction thickness [38] of 1.4 nm and relative permittivity of lipid apolar fraction of 3 [39]. As a result the specific capacitance of a defect-free bilayer on Hg should be 0.9 μF cm^{-2}. If the bilayer is supported on an ultra-thin layer of electrolyte, the total specific capacitance which is the combination of two capacitors in series will be less than the lowest value of specific capacitance i.e < 0.9 μF cm^{-2}. The increased value of C_{sp} of the DOPC bilayer indicates that at these negative applied potentials the total specific capacitance is the the sum of two specific capacitances in parallel. Indeed the specific capacitance of a water layer of thickness of the hydrophobic region of a bilayer of 2.8 nm and of relative permittivity 78 [40] is ~25 μF cm^{-2}. The previous AFM study [17] showed a bilayer structure at these potentials to have ~ 95% coverage thus a linear combination of 5% of 25 μF cm^{-2} and 95% of 0.9 μF cm^{-2} gives a specific

capacitance of the bilayer on Hg as 2.1 μF cm^{-2} which is less than half of that observed. This could be due to errors in the previous coverage estimation [17] and also in the extrapolation of the capacitance model to molecular dimensions. Indeed other studies of specific capacitances of non-covalently metal supported bilayers show values of 9 [41] for dimyristoyl phosphatidylserine (DMPS), of 3 [42] for dimyristoyl phosphatidylethanolamine (DMPE) and, of 8 [43] μF cm^{-2} for DMPC-cholesterol; bilayers on gold. In any case the capacitance results in this paper indicate that the bilayer contains water and ions with higher mean relative permittivity than the lipid apolar fraction. The increase in C_{sp} from 5 to 7.5 μF cm^{-2} from -1.1V to -1.3V indicates an increase of electrolyte in the layer with increase in applied negative potential.

The lowest value of R_{sp} at -1.1 V of $10^{4.8}$ Ω cm^2 for the bilayer on Hg is somewhat lower than that recorded for lipid bilayers of $> 10^5$ [44] and 10^6 to 10^8 [45] Ω cm^2 and in this study this decreases exponentially by two orders of magnitude with increase in applied negative potential. The presence of electrolyte in the bilayer is confirmed by a finite increased permeability to Zn^{2+} which increases with increase in applied negative potential. This is commensurate with an increase in C_{sp} and decrease in R_{sp} with increase in applied negative potential. Clearly water and electrolyte ions are drawn into the bilayer with increase in negative potential. At the potential characterising the cathodic capacitance peak current which represents the collapse of bilayer to monolayer, there are definite changes such as decrease in permeability to Zn^{2+}, increase in resistance to electrolyte and a perturbation in the bilayer capacitance. With reference to the anodic capacitance peak current and the effect of the LUDOX SM30 SiO_2 nanoparticles on it's potential, it is already established that these nanoparticles adsorb on the polar heads of DOPC mono- and bilayers [36,37]. This adsorption of SiO_2 on the layer surface must stabilise the layer structure and lower the activation energy of the transition state in bilayer reformation. Such a process would accelerate the bilayer reformation process and decrease the hysteresis between the bilayer breakdown and bilayer reformation current peaks as well as increasing the stability of the bilayer.

The structure of the bilayer with incorporated electrolyte is of interest. Burgess [46] has recorded that in the DMPC-cholesterol bilayer on gold electrodes, the water content increases with increased applied negative potential. In Burgess' study [46] the bilayer is supported on a bed of positive counter ions. Indeed Burgess' paper showed that with increasing charge density, water and ions accumulated next to the electrode with the result that the lipid film at first swelled up and then lifted off the electrode at very negative charge density. More recent studies of DMPC-cholesterol bilayers on gold [47] indicated that water penetrated deeply into the bilayers at intermediate charge densities of ~ 10 μC cm^{-2} and multimers of water molecules were detected in the bilayer. The previous modelling investigation of phospholipid on a metal electrode [18,19] proposed the bilayer rested on a bed of positive ions at negative applied potentials and at increasing charge density water and ions penetrated the layer with an accumulation of counterions on the electrode.

In the case of DOPC bilayers on Hg it was shown directly by AFM there were random physical defects in the bilayer [17] which led to 95% coverage. However the bilayer thickness remained constant with increasing applied field and at -1.3 V, the bilayer film collapsed to a monolayer with very much higher density. The containment of electrolyte in defined pores in the bilayer within an electric field at potentials up to -1.3 V is consistent with this and such structures have been simulated [48,49] and experimentally demonstrated in electric field [49] previously. The impedance analysis of the bilayer in this study shows a well ordered potential activated movement of electrolyte in the layer representing the well defined additional capacitative element. Clearly further work needs to be done to define the structure more precisely. In order to use these bilayers as a unique biomembrane model, methods can be developed through the addition of for example cholesterol to decrease the permeability of these bilayers to water and ions so that protein ion channels can be incorporated in the systems. The bilayers can also be deposited on the wafer-in-

flow cell platform [50] and used as a sensing element with bilayer spanning protein recognition elements.

5. Conclusion

1. DOPC bilayers on Hg are stable between potentials -1.0 and -1.3 V and show a characteristic capacitive current peak at ~ -1.3 V due to a bilayer breakdown which is reversed anodically with considerable hysteresis. This hysteresis is significantly decreased in a stepwise manner through adsorption of SiO_2 nanoparticles on the bilayer surface which stabilise the bilayer.

2. The bilayers on Hg are significantly less permeable to Zn^{2+} at less negative potentials between -1.1 to -1.2 V compared to a monolayer and uncoated Hg electrode but their permeability increases at higher negative potentials between -1.3 to -1.4 V.

3. Impedance analysis of the bilayer shows an additional capacitative element which becomes resolved with increase in applied negative potential. This additional capacitative element can be identified with electrolyte movement in the bilayer.

4. Measurements of bilayer specific capacitance are 5 increasing to 7.5 $\mu F\ cm^{-2}$ at -1.3 V indicating the presence of water and ions within the layer. Bilayer specific resistance decreases exponentially with increase in applied negative potential to a minimum at -1.3 V showing an increase in the bilayer permeability to electrolyte.

5. Earlier direct characterisation using AFM force-distance analysis and the present voltammetric and impedance analysis point to the bilayers containing pores allowing for electrolyte permeability within electric field.

6. Acknowledgements.

AR was funded by the Commonwealth Scholarship Commission. AV was funded by NERC (UK) Grant NE/K00686X/1. AN was funded latterly by the EU HORIZON 2020 HISENTS programme grant agreement number 685817.

7. References

[1] H.H.Zepik, P. Walde, E. L. Kostoryz, J. Code, D.M. Yourtee Lipid vesicles as membrane models for toxicological assessment of xenobiotics, Critical reviews in toxicology 38 (2008) 1-11.

[2] P.J. Beltramo, R. Van Hooghten, J.Vermant, Millimeter-area, free standing, phospholipid bilayers, Soft Matter 12 (2016) 4324-4331.

[3] R. Naumann, S.M. Schiller, F. Giess, B. Grohe, K.B. Hartman, I. Kärcher, I. Köper, J. Lübben, K. Vasilev, W. Knoll, Tethered lipid bilayers on ultraflat gold surfaces, Langmuir, 19 (2003) 5435-5443.

[4] A.L. Plant, Self-assembled phospholipid/alkanethiol biomimetic bilayers on gold, Langmuir, 9 (1993) 2764-2767.

[5] R.P. Richter, A.R. Brisson, Following the formation of supported lipid bilayers on mica: a study combining AFM, QCM-D, and ellipsometry. Biophysical Journal 88 (2005) 3422-3433.

[6] M. Heim, G. Cevc, R. Guckenberger, H.F. Knapp, W. Wiegräbe, Lateral electrical conductivity of mica-supported lipid bilayer membranes measured by scanning tunneling microscopy, Biophysical Journal 69 (1995) 489-497.

[7] L. Becucci, M.R. Moncelli, R. Naumann, R. Guidelli, Potassium ion transport by valinomycin across a Hg-supported lipid bilayer, Journal of the American Chemical Society 127 (2005) 13316-13323.

[8] L. Becucci, M.R. Moncelli, R. Guidelli, Impedance spectroscopy of OmpF porin reconstituted into a Hg-supported lipid bilayer, Langmuir 22 (2006) 1341-1346.

[9] L. Becucci, R. Guidelli, C. Peggion, C. Toniolo, M.R. Moncelli, Incorporation of channel-forming peptides in a Hg-supported lipid bilayer, Journal of Electroanalytical Chemistry576 (2005) 121-128.

[10] L. Becucci, R. Guidelli, C.B. Karim, D.D. Thomas, G. Veglia, An electrochemical investigation of sarcolipin reconstituted into a mercury-supported lipid bilayer. Biophysical Journal, 93 (2007) 2678-2687.

[11] L. Becucci, R.R. León, M.R. Moncelli, P. Rovero, R. Guidelli, Electrochemical investigation of melittin reconstituted into a mercury-supported lipid bilayer, Langmuir 22 (2006) 6644-6650.

[12] F.T. Buoninsegni, R. Herrero, M.R. Moncelli, Alkanethiol monolayers and alkanethiol| phospholipid bilayers supported by mercury: an electrochemical characterization, Journal of Electroanalytical Chemistry, 452 (1998) 33-42.

[13] M. Moncelli, L. Becucci, S.M. Schiller, Bioelectrochemistry, Tethered bilayer lipid membranes self-assembled on mercury electrodes, 63 (2004) 161-167.

[14] J.C. Munro, C.W. Frank, In situ formation and characterization of poly(ethylene glycol)-supported lipid bilayers on gold surfaces, Langmuir 20 (2004) 10567-10575.

[15] C. Peggion, F. Formaggio, C. Toniolo, L. Becucci, M.R. Moncelli, R. Guidelli, A peptide-tethered lipid bilayer on mercury as a biomimetic system, Langmuir 17 (2001) 6585-6592.

[16] A. Nelson, A. Benton, Phospholipid monolayers at the mercury/water interface, Journal of Electroanalytical Chemistry and Interfacial Electrochemistry 202 (1986) 253-270.

[17] A. Vakurov, M. Galluzzi, A. Podestà, N. Gamper, A.L. Nelson, S.D. Connell, Direct characterization of fluid lipid assemblies on mercury in electric fields, ACS nano 8 (2014) 3242-3250.

[18] A.V. Brukhno, A. Akinshina, Z. Coldrick, A. Nelson, S. Auer, Phase phenomena in supported lipid films under varying electric potential, Soft Matter 7 (2011) 1006-1017.

[19] F. A. M. Leermakers, A. Nelson, Substrate-induced structural changes in electrode-adsorbed lipid layers: a self-consistent field theory, Journal of Electroanalytical Chemistry and Interfacial Electrochemistry 278 (1990) 53-72.

[20] A. Nelson, Electrochemical analysis of a phospholipid phase transition, Journal of Electroanalytical Chemistry 601 (2007) 83-93.

[21] A. Nelson, Electrochemistry of mercury supported phospholipid monolayers and bilayers, Current Opinion in Colloid and Interface Science 15 (2010) 455-466.

[22] A. Nelson, N. Auffret, Phospholipid monolayers of dioleoyl lecithin at the mercury/water interface, Journal of Electroanalytical Chemistry and Interfacial Electrochemistry 244 (1988) 99-113.

[23] A. Nelson, N. Auffret, J. Borlakoglu, Interaction of hydrophobic organic compounds with mercury adsorbed dioleoylphosphatidylcholine monolayers, Biochimica et Biophysica Acta (BBA)-Biomembranes 1021 (1990) 205-216.

[24] A.J. Bard, L. R. Faulkner, J. Leddy, C. G. Zoski, Electrochemical methods: fundamentals and applications, Vol. 2., Wiley, New York, 1980.

[25] D. Macdonald, Transient techniques in electrochemistry, Springer Science and Business Media, 2012.

[26] C. Whitehouse, R. O'Flanagan, B. Lindholm-Sethson, B. Movaghar, A. Nelson, Application of electrochemical impedance spectroscopy to the study of dioleoyl phosphatidylcholine monolayers on mercury, Langmuir 20 (2004) 136-144.

[27] C. D.Whitehouse, D. Gidalevitz, M. Cahuzac, Roger E. Koeppe, A. Nelson. Interaction of gramicidin derivatives with phospholipid monolayers, Langmuir 20 (2004) 9291-9298.

[28] J. Merrifield, J. Tattersall, M. Bird, A.Nelson, Interaction of bispyridinium compounds with phospholipid layers in presence and absence of electric field, Electroanalysis 19 (2007) 272-279.

[29] G. Brug, A. Van Den Eeden, M. Sluyters-Rehbach, J. Sluyters, The analysis of electrode impedances complicated by the presence of a constant phase element, Journal of Electroanalytical Chemistry and Interfacial Electrochemistry 176 (1984) 275-295.

[30] S. Zhang, A. Nelson, Z. Coldrick, R. Chen, The effects of substituent grafting on the interaction of pH-responsive polymers with phospholipid monolayers, Langmuir 27 (2011) 8530-8539.

[31] P. Fruebing, Advanced lab experiments; Institute of Physics, University of Potsdam: Potsdam, Germany, 2002, pp 1-21.

[32] D. Bizzotto, A. Nelson, Continuing electrochemical studies of phospholipid monolayers of dioleoyl phosphatidylcholine at the mercury− electrolyte interface, Langmuir 14 (1998) 6269-6273.

[33] S. Kariuki, H. D. Dewald, Evaluation of diffusion coefficients of metallic ions in aqueous solutions, Electroanalysis 8 (1996) 307-313.

[34] J. Buffle, Z. Zhang, K. Startchev, Metal flux and dynamic speciation at (bio) interfaces. Part I: Critical evaluation and compilation of physicochemical parameters for complexes with simple ligands and fulvic/humic substances, Environmental Science and Technology 41 (2007) 7609-7620.

[35] N. S. Hush, J. Blackledge, Mechanism of the ZnII/Zn (Hg) exchange: Part 1: the $Zn^{2+/}$Zn (Hg) exchange, Journal of Electroanalytical Chemistry (1959) 5 (1963) 420-434.

[36] A. Vakurov, R. Brydson, A. Nelson, Electrochemical modeling of the silica nanoparticle–biomembrane interaction, Langmuir 28 (2011) 1246-1255.

[37] S. Zhang, A.Nelson, P.A. Beales, Freezing or wrapping: the role of particle size in the mechanism of nanoparticle–biomembrane interaction, Langmuir 28 (2012) 12831-12837.

[38] Y. Guo, S. Pogodin, V. A. Baulin, General model of phospholipid bilayers in fluid phase within the single chain mean field theory, The Journal of Chemical Physics 140 (2014) 05B604_1.

[39] G. Gramse, A. Dols-Perez, M. A. Edwards, Laura Fumagalli, G. Gomila, Nanoscale measurement of the dielectric constant of supported lipid bilayers in aqueous solutions with electrostatic force microscopy. Biophysical Journal 104 (2013) 1257-1262.

[40] C. G. Malmberg, A. A. Maryott, Dielectric constant of water from 0^{o} to 100^{o} C, Journal of Research of the National Bureau of Standards 56 (1956) 1-8.

[41] E. Madrid, S. L. Horswell, Effect of headgroup on the physicochemical properties of phospholipid bilayers in electric fields: size matters, Langmuir 29 (2013) 1695-1708.

[42] E. Madrid, S. L. Horswell, Effect of electric field on structure and dynamics of bilayers formed from anionic phospholipids, Electrochimica Acta 146 (2014) 850-860.

[43] X. Bin, I. Zawisza, J. D. Goddard, J. Lipkowski, Electrochemical and PM-IRRAS studies of the effect of the static electric field on the structure of the DMPC bilayer supported at a Au (111) electrode surface, Langmuir 21 (2005) 330-347.

[44] M. Naumowicz, Z.A.Figaszewski, Pore formation in lipid bilayer membranes made of phosphatidylcholine and cholesterol followed by means of constant current, Cell biochemistry and Biophysics 66 (2013): 109-119.

[45] M.Montal, P. Mueller, Formation of bimolecular membranes from lipid monolayers and a study of their electrical properties, Proceedings of the National Academy of Sciences, 69 (1972) 3561-3566.

[46] I. Burgess, M. Li, S. L. Horswell, G. Szymanski, J. Lipkowski, J. Majewski, S. Satija, Electric field-driven transformations of a supported model biological membrane—an electrochemical and neutron reflectivity study, Biophysical journal 86 (2004) 1763-1776.

[47] T.Uchida, M. Osawa, J. Lipkowski, SEIRAS studies of water structure at the gold electrode surface in the presence of supported lipid bilayer, Journal of Electroanalytical Chemistry 716 (2014) 112-119.

[48] H. Leontiadou, A.E.Mark, S. J. Marrink, Molecular dynamics simulations of hydrophilic pores in lipid bilayers, Biophysical Journal 86 (2004) 2156-2164.

[49] F. Dehez, L. Delemotte, P. Kramar, D. Miklavčič, M.Tarek, Evidence of conducting hydrophobic nanopores across membranes in response to an electric field, The Journal of Physical Chemistry C 118 (2014) 6752-6757.

[50] S. Mohamadi, D. Tate, A.Vakurov, A. Nelson, Electrochemical screening of biomembrane-active compounds in water, Analytica Chimica Acta 813 (2014) 83-89.

Figure captions.

Figure 1

Capacitance current (-I) versus potential (-E) plots of DOPC coated HMDE in 0.1 mol dm^{-3} KCl with 0.001 mol dm^{-3} phosphate buffer (pH 7.4) measured by RCV at 40 Vs^{-1}; (a) in potential range -0.2 to -1.6 V (black) and -0.9 to -1.6 V prior to (red) decreasing the electrode area to form bilayer and following (green) increasing the electrode area to restore monolayer, and (b) in potential range -0.9 to -1.6 V for the bilayer configuration. All currents normalised to electrode area 0.0088 cm^2.

Figure 2

Equivalent circuit representing eqn [3] where R_m is resistance of bilayer on electrode.

Figure 3

(a) Cathodic capacitance current (-I) versus experimental electrode area (A) plots measured by RCV at 40 V s^{-1} at -1.07 V in 0.1 mol dm^{-3} KCl with 0.001 mol dm^{-3} phosphate buffer (pH 7.4) and (b) Zn^{2+} reduction current versus experimental electrode area sampled at 30 ms following potential pulse from -0.9 to -1.1V at DOPC bilayer on HMDE in same electrolyte as (a) without phosphate buffer. All currents normalised to electrode area 0.0088 cm^2.

Figure 4

(a) Plot of -I vs $t^{-1/2}$ of Zn^{2+} reduction transient following pulse from -0.85 to -1.1V at uncoated HMDE and, (b) Sampled current voltammograms at 30 ms derived from Zn^{2+} reduction transients following pulse from -0.85 to, -1.1 to -1.6 V at uncoated HMDE (black filled circle) and DOPC

monolayer (blue open triangle) and DOPC bilayer (red filled triangle) coated HMDE in 0.1 mol dm^{-3} KCl containing 0.2 mmol dm^{-3} Zn(II). All currents normalised to electrode area 0.0088 cm^2.

Figure 5

Zn^{2+} reduction current transients following voltage pulse from -0.85V to potentials shown in each figure at DOPC bilayer coated HMDE (red) with corresponding fits (black) to eqn [2] in 0.1 mol dm^{-3} KCl containing 0.2 mmol dm^{-3} Zn(II).

Figure 6

Impedance data transformed to complex capacitance plane derived from impedance measurements at DOPC bilayer coated HMDE in 0.1 mol dm^{-3} KCl with 0.001 mol dm^{-3} phosphate buffer (pH 7.4) at potentials indicated on the diagrams of imaginary versus real specific capacitance. Data are represented by cross and eqn [3] fits are the solid red lines.

Figure 7

(a) α, (b) β and (c) C_{sp} values derived from, fits to complex capacitance data using eqn [3] for the DOPC bilayer on Hg as a function of the potential and, eqn [4] for extraction of C_{sp} values.

Figure 8

(a) Heterogenous rate constant (k_f) of Zn^{2+} reduction at DOPC bilayer on HMDE in 0.1 mol dm^{-3} KCl with 0.2 mmol dm^{-3} Zn^{2+} derived from fits of eqn [2] to transients in Figure 5 and (b) Specific bilayer resistance (R_{sp}), derived from τ and (C_s-C) extracted from fits to complex capacitance data in Figure 5 using, eqns [3] and [5] respectively, plotted as a function of potential.

Figure 9

Capacitance current (-I) versus potential (-E) plots measured by RCV at 40 Vs^{-1} in potential range -0.9 to -1.6 V of DOPC bilayers deposited on HMDE in 0.1 mol dm^{-3} KCl with 0.001 mol dm^{-3} phosphate buffer at pH 7.4 without (black) and with 0.0012 % of Ludox SM-30 silica nanoparticles (14 nm diameter) after 45 s (blue) and 200 s (red) exposure time. All currents normalised to electrode area 0.0088 cm^2.